JOURNAL OF AIRCRAFT
Vol. 39, No. 5, September–October 2002

Recent Improvements to a Hybrid Method for Rotors in Forward Flight

Zhong Yang,* Lakshmi N. Sankar,† Marilyn J. Smith,‡ and Oliver Bauchau§
Georgia Institute of Technology, Atlanta, Georgia 30332-0150

A hybrid Navier–Stokes/full potential solver has been developed for the efficient prediction of three-dimensional unsteady viscous flow phenomena that occur over helicopter rotors in forward flight. The method combines a Navier–Stokes analysis near the blade, modeling the viscous flow and near wake with a potential flow analysis in the far field, modeling inviscid isentropic flow. A grid motion module has been developed to account for the blade motion and elastic deformations. Free and prescribed wake models have been developed to account for the tip vortex effects once the vortex leaves the viscous flow region and enters the potential flow region. Sample results are presented for a two-bladed AH-1G rotor in descent and for a UH-60A rotor in high-speed forward flight. Comparisons with experiments, flight test data, and other numerical simulations are given.

Nomenclature

A, B, C	=	transformation matrices
a	=	speed of sound
C_l	=	sectional lift coefficient
C_n	=	sectional normal coefficient
C_p	=	pressure coefficient
C_T	=	rotor thrust coefficient
c	=	chord
$\mathrm{d}(\,)/\mathrm{d}t, \partial(\,)/\partial t$	=	ordinary and partial derivatives with respect to time
E_i, E_V	=	inviscid and viscous flux, respectively
e	=	total energy per unit volume
J	=	Jacobian of transformation
k_{match}	=	interface surface normal coordinate
k_T	=	turbulent thermal conductivity
k_x, k_y	=	inflow coefficients in x and y coordinate directions
M	=	Mach number
M_{tip}	=	tip Mach number
$\boldsymbol{n}$	=	unit normal vector to the surface
p	=	pressure
$\boldsymbol{q}$	=	vector of conserved flow variables
R	=	blade radius
Re	=	Reynolds number
r	=	radial distance from the rotor hub
S	=	surface of the control volume
T	=	transformation matrix
t	=	time, also Eulerian angles in Eq. (6)
U, V, W	=	contravariant component of velocity
u, v, w	=	Cartesian components of velocity
u_w, v_w, w_w	=	induced velocity components due to the wake
V_w	=	induced total velocity due to the wake
x, y, z	=	Cartesian coordinates
$\boldsymbol{x}$	=	vector of Cartesian coordinates
α	=	angle of attack
α_{tpp}	=	tip path plane angle
β_0	=	coning angle
β_{1c}, β_{1s}, etc.	=	cyclic flapping coefficients
Γ	=	bound circulation, tip vortex strength
γ	=	ratio of specific heats
Θ_0	=	collective pitch angle
Θ_{1c}, Θ_{1s}, etc.	=	cyclic pitch coefficients
λ	=	inflow velocity with Cartesian components $(\lambda_x, \lambda_y, \lambda_z)$
μ	=	advance ratio
ξ, η, ζ	=	curvilinear coordinates
σ	=	rotor solidity
ρ	=	density
ϕ	=	velocity potential
ψ	=	azimuthal angle
Ω	=	rotor rotational speed, also control volume in Eq. (1)
ω	=	vorticity
$\nabla\phi$	=	disturbance velocity potential

Subscripts

b	=	bound
FP	=	associated with full potential zone
i, j, k	=	grid indices
NS	=	associated with the Navier–Stokes zone
n	=	normal
PM	=	pitching moment
RM	=	rolling moment
x, y, z, t	=	partial derivative
∞	=	freestream condition

Presented as Paper 2000-0260 at the AIAA 38th Aerospace Sciences Meeting and Exhibit, Reno, NV, January 2000; received 16 March 2001; revision received 16 June 2002; accepted for publication 15 June 2002.

*Graduate Research Assistant, School of Aerospace Engineering.
†Regent's Professor, School of Aerospace Engineering. Associate Fellow AIAA.
‡Assistant Professor, School of Aerospace Engineering. Associate Fellow AIAA.
§Professor, School of Aerospace Engineering. Senior Member AIAA.

Introduction

THE prediction of rotor blade aerodynamic loads, especially in forward flight, requires accurate and efficient modeling of several distinct phenomena. On the advancing side, the combination of rotational speed and forward-flight velocity may cause the flow in the tip region to be transonic, with the formation of supersonic pockets and shock waves. Because the inboard section of the retreating blade operates in a reversed flow condition, the outboard stations are required to operate at higher angles of attack to generate sufficient lift. This may cause dynamic stall. Strong tip vortices in the rotor wake dominate the flowfield and produce an unsteady and nonuniform induced velocity field at the rotor disk. Finally, rapid one-per-revolution and two-per-revolution variations may cause structural bending and torsional deformations, which must be properly modeled.

Historically, helicopter industries have used comprehensive helicopter analyses to model rotors in forward flight. These analyses contain phenomenological models for the blade aerodynamics and the wake coupled to simple structural dynamics and trim models. Notable among the comprehensive helicopter analyses is the CAMRAD family of codes by Johnson.[1,2]

During the early 1980s, computers became powerful enough to model helicopter aerodynamics using finite difference potential flow methods. In these methods, the near wake is modeled as a vortex sheet across which the velocity potential is discontinuous. The effect of the far wake is typically computed from an external wake model and introduced as an angle-of-attack correction. Trim is also achieved externally and fed back into analysis. For example, the FDR code by Chattot[3] was coupled to a comprehensive code. The effect of the wake and trim was input to the solver as a table of angle-of-attack changes. Sankar and Prichard,[4] Strawn and Caradonna,[5] Strawn and Tung,[6] and Strawn et al.[7] have developed unsteady full potential flow solvers, RFS2 and FPR. In these analyses, the flow results were coupled to CAMRAD in an open-loop fashion. Sankar and Tung[8] have also coupled a three-dimensional Euler solver for rotors to the CAMRAD code and shown encouraging results.

Because the rotor wake has a substantial effect on the blade aerodynamics, in current generation computational fluid dynamics (CFD) analyses the wake is modeled from first principles. Steinhoff and Ramachandran,[9,10] Ramachandran et al.,[11] and Ramachandran and Caradonna[12] applied a vorticity embedding technique in conjunction with a potential flow analysis to model the wake. A hover version of their method is called HELIX-I, and a forward-flight version (HELIX-II) has been developed.

Most, if not all, current generation Euler or Navier–Stokes solvers are capable of capturing the rotor wake as a part of the solution. Srinivasan and Baeder developed one of the first Navier–Stokes analyses capable of capturing the wake of a hovering rotor.[13] Hariharan developed a fifth-order essentially nonoscillatory (ENO) scheme and applied it to rotors in hover and rotor–airframe interactions.[14] Bangalore and Sankar[15] studied a UH-60A configuration and a rotor equipped with a leading-edge slat in forward flight. Ahmad and Duque[16] have also solved forward-flight flowfields using a version of the NASA Ames Research Center code OVERFLOW, with an embedded overset grid technique. Their calculations used information regarding the blade dynamics from the flight-test or wind-tunnel data. Bauchau and Ahmad[17] accounted for the blade elastic deformations by tightly coupling the CFD code OVERFLOW with a computational structural dynamics code called DYMORE.

Despite these advances, the blade loads prediction capability and the solution efficiency of the current generation of rotor CFD analyses are not at a level acceptable to the helicopter industry. The usefulness of these analyses is limited because the rotor is not trimmed, because the tip vortex capturing suffers from excessive numerical diffusion, and because the blade dynamics and aeroelasticity are not adequately modeled. Euler/Navier–Stokes simulations require significant computational memory and time, often consuming weeks of CPU time to map the flight regime of interest.

Hybrid methodologies attempt to alleviate these deficiencies in the following manner. Navier–Stokes analyses are applied only in the unsteady viscous flow regions near the blades. All other regions where viscous effects are minimal are modeled using a potential flow analysis or a Lagrangian wake model. Berezin and Sankar[18] developed such a hybrid rotor solver and applied it to a UH-60A rotor in forward flight. Only the near wake was captured from first principles. This scheme was coupled to a comprehensive code called RDYNE[19] that properly accounted for the far wake and the trim effects. Berkman et al.[20] improved this hybrid technique by modeling the entire wake from first principles, using a combination of vortex capturing and a Lagrangian wake model; they obtained good correlation in hover. Mello[21] found that computational savings using these hybrid methods are dependent on the physics of the flow, as well as on the size of the computational domain and the type of computer utilized to solve the problem. For problems with large separation, the viscous/inviscid boundary must move farther away from the structure, requiring a larger area to be solved using Navier–Stokes solvers. For more moderate unsteady cases where the boundary is closer, CPU savings of up to 40% were observed on workstations for the same grid size. Moulton et al.[22–24] coupled the HELIX-I analysis to the rotor Navier–Stokes solver TURNS and modeled rotors in hover. Bangalore et al. extended this methodology to forward flight through the use of an overset grid method.[25] In many of these calculations, the rotor was not trimmed, and the elastic effects were not accounted for.

Scope of the Present Work

The object of this research is to develop an efficient rotor flow solver that will accurately predict the aerodynamic loads on a rotor in forward flight. To ensure that the proper physics are modeled, the methodology should include a trim process, have a self-consistent wake model, and should properly account for the aeroelastic deformations of the blade. This method is an extension of the hybrid method discussed in Refs. 18 and 20.

Mathematical Formulation

The mathematical and numerical formulations are well developed and have been extensively published.[15,18] Therefore, only a brief description of the method is given here. As discussed earlier, the hybrid method combines a compressible Navier–Stokes solver for modeling the viscous flow near the blade surface and the near wake, a compressible full-potential flow solver for modeling the inviscid flow regions far away from blade, and a Lagrangian wake model for the far-wake effect, as depicted in Fig. 1.

Viscous Zone

The Navier–Stokes equations over a deforming grid may be written in finite volume form as

$$\frac{\partial}{\partial t}\iiint_{\Omega} \boldsymbol{q}\,\mathrm{d}\Omega + \oiint_{S} (\boldsymbol{E}_I - q\boldsymbol{V}_{\text{grid}})\cdot \boldsymbol{n}\,\mathrm{d}S = \oiint_{S} \boldsymbol{E}_V \cdot \boldsymbol{n}\,\mathrm{d}S \quad (1)$$

The grid velocity terms V_{grid} take into account that the cell faces are moving with respect to an inertial observer or deforming as a result of aeroelastic effects. The inviscid fluxes are computed using an upwind scheme. In the present code, these terms can be computed to third- or fifth-order spatial accuracy using an ENO scheme described in Ref. 14. At each time step, the discretized nonlinear algebraic equations are linearized about the preceding time step. The resulting sparse heptadiagonal matrix system is solved using an approximate factorization scheme. The Baldwin–Lomax eddy viscosity model is used to model effects of turbulence within the viscous region.

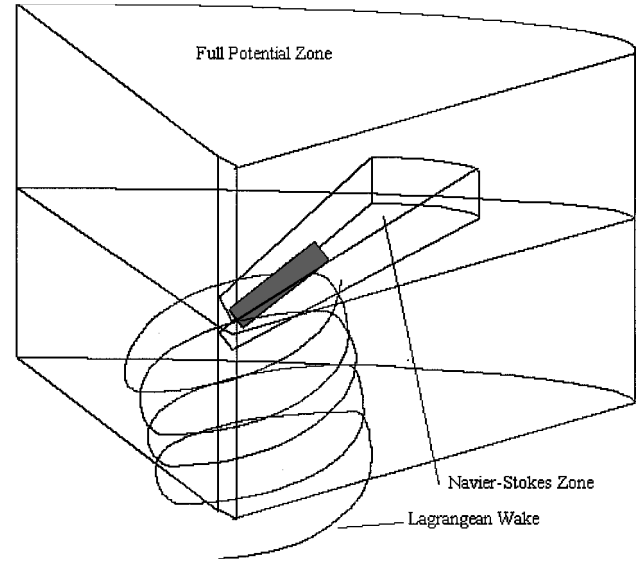

Fig. 1 Hybrid grid configuration for the current rotor application.

Potential Flow Zone

The potential flow zone is solved using the continuity equation

$$\frac{\partial}{\partial t}\iiint_{\Omega}\rho\,\mathrm{d}\Omega+\iint_{S}\rho(\boldsymbol{V}-\boldsymbol{V}_{\mathrm{grid}})\cdot\boldsymbol{n}\,\mathrm{d}S=0 \tag{2}$$

where the flow velocity V is made up of three components: freestream velocity, disturbance potential velocity, and induced velocity caused by the far wake.

$$V=V_{\infty}+\nabla\phi+V_{w} \tag{3}$$

The density is coupled to the velocity field by the isentropic form of the energy equation. A three-dimensional unsteady compressible potential flow analysis developed by Sankar et al.[26] is used. This solver uses a three-factor alternating direction implicit scheme.

Interface Between the Full-Potential and Navier–Stokes Zones

The interface separating the Navier–Stokes zone from the full-potential zone must be carefully handled to allow three type of waves (acoustic, vorticity, and entropy waves) to propagate out to the far field without false reflections. The equations to handle these interfaces accurately were originally developed by Sankar et al.[27] and verified in Ref. 18. They are summarized here for completeness. At the interface, the five components of the flow properties for the Navier–Stokes equations are computed directly from the full-potential domain. The zones overlap by one full cell on either side of the match line. The velocity components are found by adding potential and wake-induced velocities. For example, at the $k=k_{\mathrm{match}}$ interface shown in Fig. 2, the flowfield variables are computed using the formulations

$$u_{i,j,k_{\mathrm{match}}}=(\phi_x)_{i,j,k_{\mathrm{match}}}+u_w,\qquad v_{i,j,k_{\mathrm{match}}}=(\phi_y)_{i,j,k_{\mathrm{match}}}+v_w$$

$$w_{i,j,k_{\mathrm{match}}}=(\phi_z)_{i,j,k_{\mathrm{match}}}+w_w,\qquad \rho/\rho_{\infty}=\left(a^2/a_{\infty}^2\right)^{1/(\gamma-1)}$$

$$e=\rho[a^2/\gamma(\gamma-1)+V^2/2] \tag{4}$$

The local a can be determined from the energy equation

$$a^2=a_{\infty}^2+[(\gamma-1)/2]\left(V_{\infty}^2-V^2-2\phi_t\right) \tag{5}$$

Because there is an overlap of cells at the interface, these computations would also be calculated for the $k_{\mathrm{match}-1}$ and $k_{\mathrm{match}+1}$ cells as well. The entropy wave is ignored once it leaves the inner viscous zone, consistent with the assumption of isentropy in potential flows. The vorticity is converted into vortex elements that are modeled using a Lagrangian wake model. The conservation of mass is accounted for by matching the normal component of velocity at the interface

$$v_n|_{\mathrm{NS}}=v_n|_{\mathrm{FPE}} \tag{6}$$

To minimize computational resources required for this problem, the zonal interface is allowed to change at each azimuthal location.

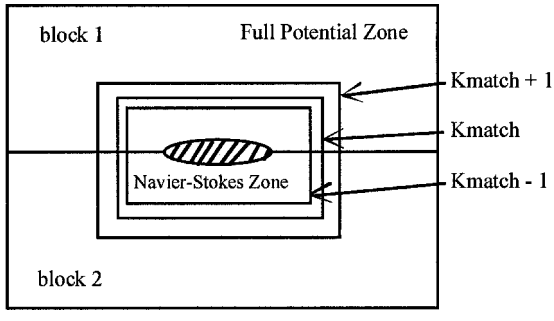

Fig. 2 Boundary conditions between the Navier–Stokes and full-potential zones.

Vorticity magnitude is utilized as the optimization parameter. The location of the zones about the blade is estimated by the user at the beginning of the computation. If the vorticity along the chosen zonal interface remains within a tolerance of vorticity magnitude, the interface location remains unchanged. If the vorticity magnitude along the plane is higher than the upper limit of the tolerance band, the interface moves away from the blade. If the vorticity magnitude is lower, the interface moves closer to the blade.

Blade Dynamics

A module for blade motion has been developed handle rigid blade motions in flap and pitch and the complex blade deformation due to aeroelastic effects. Eulerian angles[28] are a useful and convenient way of expressing the motion of rotating bodies in an inertial frame. The periodic blade motion in pitch and flap are described by a Fourier series, in terms of the blade azimuth:

$$\beta=\beta_0+\beta_{1c}\cos\psi+\beta_{1s}\sin\psi+\beta_{2c}\cos 2\psi+\beta_{2s}\sin 2\psi+\cdots$$

$$\theta=\theta_0+\theta_{1c}\cos\psi+\theta_{1s}\sin\psi+\theta_{2c}\cos 2\psi+\theta_{2s}\sin 2\psi+\cdots \tag{7}$$

Two approaches for modeling blade dynamics have been evaluated. In the first approach, the blades are assumed to be rigid. The (x, y, z) positions in space at any instance in time may be related to (x, y, z) at an earlier time through simple transformation such as

$$T=[A][B][C],\qquad \boldsymbol{x}_{\mathrm{new}}=T\boldsymbol{x}_{\mathrm{old}} \tag{8}$$

The transformation matrix T is given by the following equation in terms of the Eulerian angles:

$$T=\begin{bmatrix}t_{11} & t_{12} & t_{13}\\ t_{211} & t_{22} & t_{23}\\ t_{31} & t_{32} & t_{33}\end{bmatrix} \tag{9}$$

where

$$t_{11}=\cos\theta\cos\psi,\qquad t_{12}=\cos\beta\sin\psi+\sin\beta\sin\theta\cos\psi$$

$$t_{13}=\sin\psi\sin\beta-\cos\beta\sin\theta\cos\psi,\qquad t_{21}=-\cos\theta\sin\psi$$

$$t_{22}=\cos\beta\cos\psi-\sin\beta\sin\theta\sin\psi$$

$$t_{23}=\sin\beta\cos\psi+\cos\beta\sin\theta\sin\psi,\qquad t_{31}=\sin\theta$$

$$t_{32}=-\sin\beta\cos\theta,\qquad t_{33}=\cos\beta\cos\theta \tag{10}$$

If the blades are not rigid, this grid motion includes additional rotations (in twist) and bending deformations.

The addition of these terms requires that the motion of the blade be included in the equations of motion. There are currently two methods to achieve this end. The classical approach is to compute the new blade location in space, regenerate the grid about the blade, and include the local motion of the blade from the preceding time step through velocity terms. This final step is known as the grid conservation law and is needed to ensure that mass and momentum conservation laws are maintained in each cell. This generates a small velocity even at the surface of the blade. The alternative method for implementing blade motion is the utilization of the transpiration boundary condition. This has been successfully utilized by a number of researchers,[29,30] as long as the deflection of the surface and the time steps remained relatively small, as they are for the rotor problems discussed here. The transpiration technique does not require any new grids to be computed. Instead, the local motion of the blade surface is modeled via the new surface boundary condition:

$$(\boldsymbol{V}-\boldsymbol{V}_{\mathrm{surface}})\cdot\boldsymbol{n}=(\Omega r+V_{\infty}\sin\psi)\left(\frac{\mathrm{d}z_{\mathrm{surface}}}{\mathrm{d}x}\right)\zeta_x\Delta t \tag{11}$$

The modification of the boundary condition includes new terms on both the left and right sides of the equation. These new terms

balance the equation so that the Navier–Stokes boundary condition at the surface ($\boldsymbol{V} \cdot n = 0$) is still attained. To optimize computational resources, the transpiration velocity approach was utilized for this research.

Wake Model

In the present hybrid method, two kinds of wake models are implemented: a rigid wake model and a free wake model. In both of these models, the tip vortex is modeled as a connected series of straight-line segments. The connecting points are called "markers." The first vortex element marker is placed at the downstream interface between the Navier–Stokes and the full-potential zones. The downward drift of the tip vortex from the blade tip to the interface due to the induced velocity is also considered in placing the marker. After each marker is created, it is convected with the local velocity of the freestream plus a velocity component induced by the wake itself.

Rigid Wake Model

In the rigid wake model, The tip vortex position is described by its age ϕ, which is the current blade azimuthal angle position minus the azimuthal angle of the shedding initiation point. The wake geometry is described in the inertial coordinate system as

$$x = r\cos(\psi - \phi) + \mu_x\phi + \lambda_x\phi$$

$$y = r\sin(\psi - \phi) + \mu_y\phi + \lambda_y\phi$$

$$z = z_0 + \mu_z\phi - \lambda_z\phi \tag{12}$$

where the ψ is given for the reference blade. The Glauert uniform inflow model is used to compute the values of the inflow in the Cartesian directions.

The rigid wake model requires a negligible amount of computation, but can not model the wake distortion. If measured wake geometry information is available, then the distorted geometry can be calculated.

Free Wake Model

If the wake from the preceding blade remains close to the resolved blade, the distortion of the wake geometry can have a large effect on the loading. In the free wake model, based on the model described in Ref. 20, the convection speed of each wake marker includes the velocity induced by the wake itself. In the hybrid code, the Biot–Savart law is used to evaluate the self-induced velocity at every element in the wake. The convection velocities are numerically integrated using a one-step explicit scheme to obtain the positions of the wake markers at the next time step.

Tip Vortex Strength

In forward flight, the aerodynamic loads vary with the azimuth. The strength of the shedding tip vortex has a different value at each azimuthal position, whereas it is a single steady-state value in hover. The following procedure has been developed. At the start of the calculation, a rigid wake geometry is assumed, and the tip vortex strengths are initialized using blade element theory or a model discussed by Mello et al.[31]:

$$\Gamma_b(\boldsymbol{r}, \psi) = \Gamma_0 \boldsymbol{r}\sqrt{1 - \boldsymbol{r}^2}[1/(1 + 1.5k_T\mu\sin\psi)] \tag{13}$$

where k_T has a value of 0.982. At subsequent time levels, the peak bound circulation of the reference blade is used to define the strength of the most recently shed wake element.

Rotor Trim

Accurate aerodynamic predictions are only possible if the rotor is operating at the desired thrust level, which requires a trimming procedure. At a particular flight speed, the desired state is achieved through the adjustment of the rotor collective and cyclic pitch:

$$c_T = c_T(\theta_0, \theta_{1c}, \theta_{1s}), \qquad c_{\mathrm{PM}} = c_{\mathrm{PM}}(\theta_0, \theta_{1c}, \theta_{1s})$$

$$c_{\mathrm{RM}} = c_{\mathrm{RM}}(\theta_0, \theta_{1c}, \theta_{1s}) \tag{14}$$

where c_T, c_{PM}, and c_{RM} represent the coefficients of thrust, pitching moment, and rolling moment, respectively. The blade pitch angle is defined by the first harmonic term of the Fourier series

$$\theta(\psi) = \theta_0 + \theta_{1c}\cos\psi + \theta_{1s}\sin\psi \tag{15}$$

Because the relationship between the rotor aerodynamic parameters c_T, c_{PM}, and c_{RM} and the blade pitch angle is nonlinear, an iterative technique is necessary to obtain the convergence of the trim procedure. A Newton–Raphson iterative method is employed to trim the rotor automatically. Given an initial guess for the control settings θ_0^0, θ_{1c}^0, and θ_{1s}^0, the flow solver is first run for several blade revolutions to get the initial rotor performance parameters c_T^0, c_{PM}^0, and c_{RM}^0. The calculations are stopped, and an estimate for the changes to the control settings such as $\Delta\theta_0$ can be obtained using the Newton–Raphson iterative method:

$$\begin{Bmatrix} c_T \\ c_{\mathrm{PM}} \\ c_{\mathrm{RM}} \end{Bmatrix}^{(0)} + \begin{bmatrix} \dfrac{\partial c_T}{\partial\theta_0} & \dfrac{\partial c_T}{\partial\theta_{1c}} & \dfrac{\partial c_T}{\partial\theta_{1s}} \\ \dfrac{\partial c_{\mathrm{PM}}}{\partial\theta_0} & \dfrac{\partial c_{\mathrm{PM}}}{\partial\theta_{1c}} & \dfrac{\partial c_{\mathrm{PM}}}{\partial\theta_{1s}} \\ \dfrac{\partial c_{\mathrm{RM}}}{\partial\theta_0} & \dfrac{\partial c_{\mathrm{RM}}}{\partial\theta_{1c}} & \dfrac{\partial c_{\mathrm{RM}}}{\partial\theta_{1s}} \end{bmatrix}^{(0)} \times \begin{Bmatrix} \Delta\theta_0 \\ \Delta\theta_{1c} \\ \Delta\theta_{1s} \end{Bmatrix}^{(0)} = \begin{Bmatrix} c_T \\ c_{\mathrm{PM}} \\ c_{\mathrm{RM}} \end{Bmatrix}^{(d)} \tag{16}$$

Generally, $c_T^d = c_T^{\mathrm{supplied}}$, $c_{\mathrm{PM}}^d = 0$, and $c_{\mathrm{RM}}^d = 0$.

With these new control settings as the initial guess, the preceding iterative procedure continues until the rotor performance parameters achieve the desired value. The direct application of this trim procedure in either the Navier–Stokes or the full-potential modules takes a number of blade revolutions and becomes very expensive. Instead, the derivatives of the rotor performance parameters are computed using a simple lifting-line technique[32] external to the hybrid method after every blade revolution. By the use of the values of the performance parameters averaged at every 5-deg azimuthal location, the change in collective and cyclic pitch values can be quickly computed using lifting-line theory for the next revolution of the hybrid method. This method typically requires from three to seven revolutions of the blade to approach the desired performance values.

Results and Discussion

The hybrid analysis just described has been validated through a study of rotors in forward flight. Calculations have been computed for the AH-1G and UH-60A rotors in forward flight. An H–O multiblock grid is used. The solution is impulsively started with an assumed prescribed wake estimated from lifting-line theory, and the solution becomes repeatable from one revolution to the next in approximately three rotor revolutions.

UH-60A in Forward Flight

The UH-60A rotor blade has an aspect ratio of 15.3 and a maximum twist of 13 deg. It has a rearward sweep of 20 deg starting from 93% radius. In the experiment,[33,34] the blades were fully articulated, and the rotor had been trimmed to eliminate one-per-revolution flapping. Because the blade was soft in torsion, the elastic twist was also measured at several radial locations as a function of the blade azimuth. The instantaneous blade pitch angle (including elastic deformations) is, thus, available at each radial location. This information was used in the analysis as follows. The rigid blade motions were handled using Eq. (5). The additional rotations due to elastic deformations were modeled using a transpiration velocity approach.

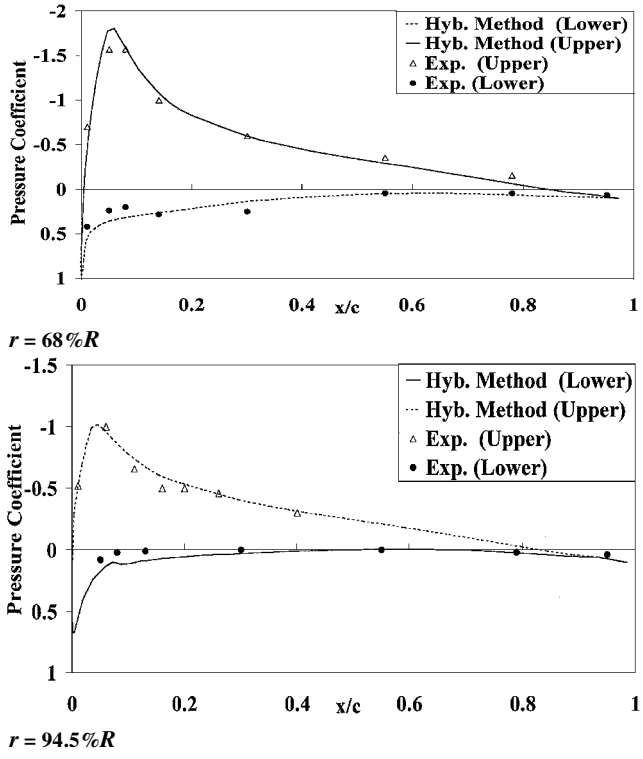

Fig. 3 Pressure coefficients at $\psi = 0$ deg for advancing UH-60A rotor.

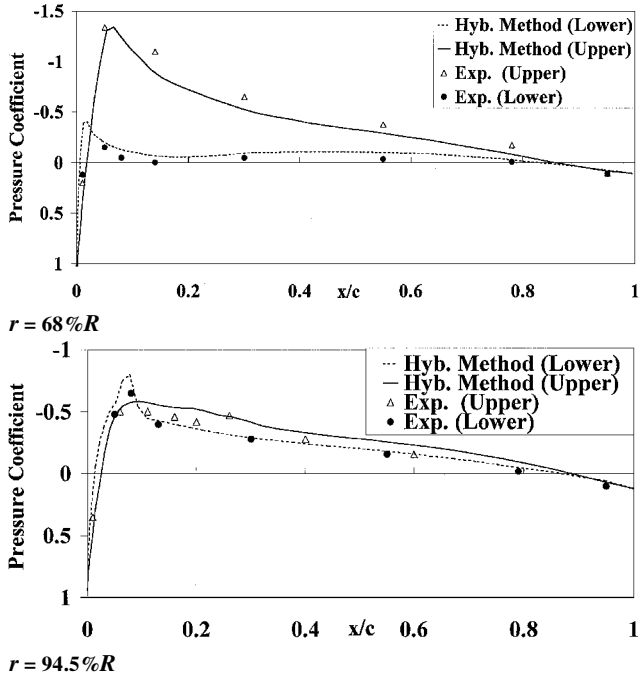

Fig. 4 Pressure coefficients at $\psi = 90$ deg for advancing UH-60A rotor.

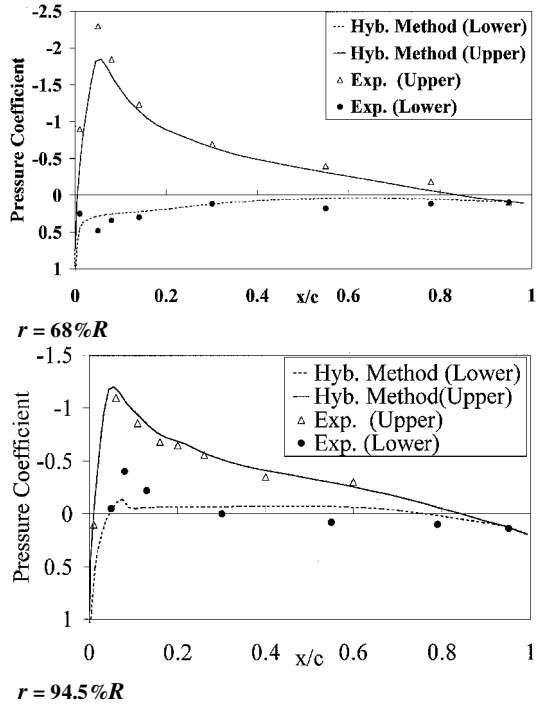

Fig. 5 Pressure coefficients at $\psi = 180$ deg for advancing UH-60A rotor.

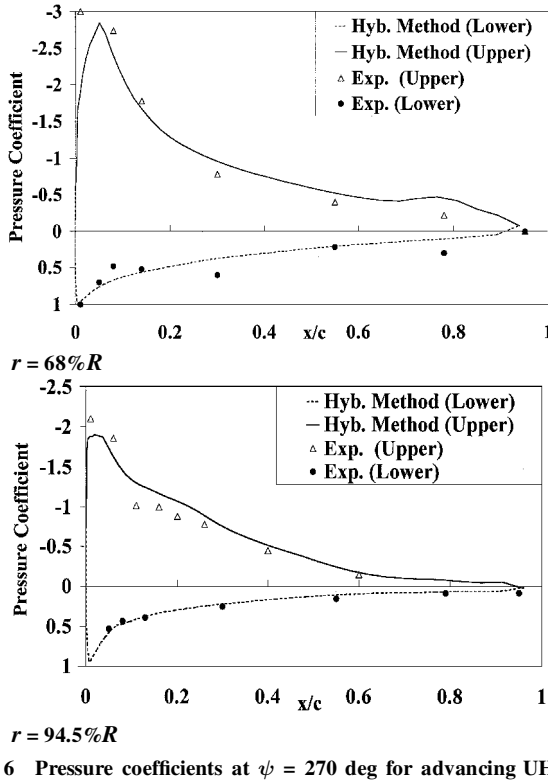

Fig. 6 Pressure coefficients at $\psi = 270$ deg for advancing UH-60A rotor.

Figures 3–6 show the surface pressure at the inboard and outboard section compared to the experimental data. At $\psi = 0$ deg the pressure inboard at 67.5%R and outboard at 94.5%R are well predicted, and the suction peaks are also captured well. Between $\psi = 90$ and 160 deg, the measured data show negative loads in the tip region because the blade is highly twisted and is pitched down. The computed results in the outboard section at 94.5%R correctly reproduce this negative lift. Regions of supersonic flow are also observed in the tip region over about 20% of the leading edge of the lower surface between $\psi = 90$ and 120 deg in the experiment. The hybrid results show a shock located at about 10% chord near the leading edge on the lower surface.

On the retreating side of the rotor, the flow is more complex. Flow separation and dynamic stall may occur, and these features usually are associated with intense turbulence. The accuracy of the transition and turbulence models is an important factor in computing such a flowfield. Because the hybrid code uses a simple algebraic turbulence model and a very coarse grid in the inboard region, there is some difficulty in capturing the measured physical phenomena. At the $\psi = 180$ deg azimuthal angle, the suction peak in the inboard region is underpredicted.

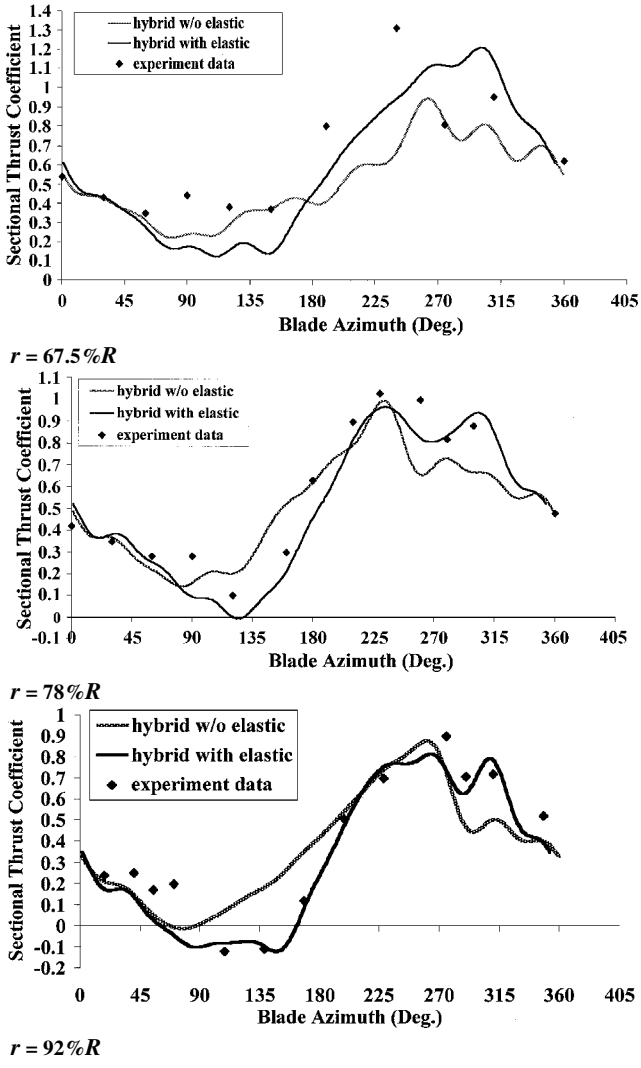

Fig. 7 Sectional thrust for UH60A at different radial locations.

The sectional thrust coefficients are shown in Fig. 7 at a number of radial locations with and without the elastic deformation effects. From the experimental data,[34] it is seen that the instantaneous loads are a strong function of the blade position, rising and falling with the blade pitch. The thrust at the inboard 67.5% span location is underpredicted in the second and third quadrants. This is believed to be due to the coarse grid in the inboard region.

At the outboard region, the thrust coefficients at 78 and 92% span compare fairly well with experimental data. The experimental data show a large increase in the thrust coefficients with azimuthal location ψ on the advancing side, and the magnitude of the thrust drop increases along the radial location to the tip. With inclusion of the elastic deformation, the negative lift is captured well, and an increase in the magnitude of the negative lift with radial distance can also be seen. This agrees with the suggestion by Ramachandran and Caradonna[12] that the negative lift is related to the blade deformation in twist and that the model rotor is undergoing a sizable nose-down twist.

AH-1G in Forward Flight

This rotor was tested as part of a operational loads survey program at NASA Ames Research Center.[35] The available data include overall instantaneous thrust coefficient C_T and the sectional normal force coefficient C_n based on an integration of the pressure data collected from pressure ports on the blade. The two-bladed teetering rotor has a rectangular planform and uses a symmetrical airfoil. The linear twist is -10 deg from root to tip. The blade has an aspect ratio of 9.8.

Table 1 H-1G blade motion

Blade Motion	θ_0	θ_{1s}	θ_{1c}	β_{1s}	β_{1c}
Experiment	6.0	−5.5	1.7	−0.15	2.13
Numerical, after trim	8.0	−6.5	2.5	−0.15	2.13

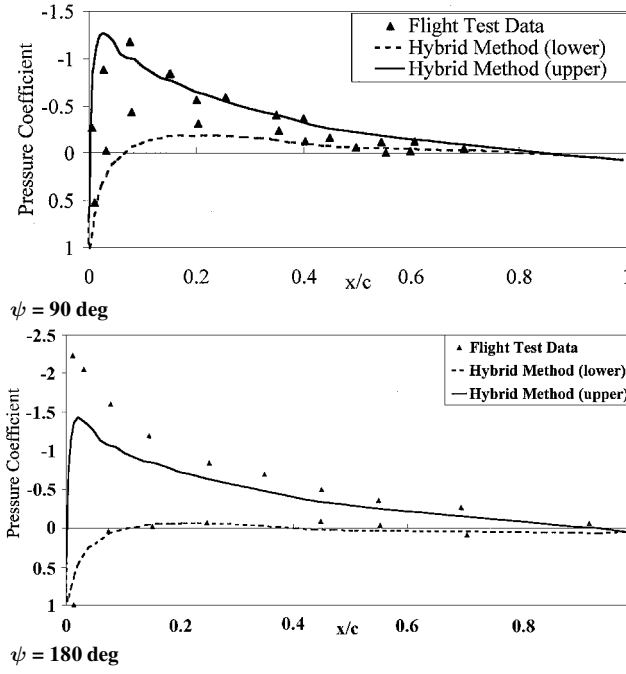

Fig. 8 Pressure coefficients at $r = 60\%R$, for advancing AH-1G rotor.

The case chosen for detailed study corresponds to flight-test data at an advance ratio of 0.19, tip Mach number (based on tip speed ΩR) of 0.65, and a time-averaged total thrust coefficient of 0.00464. The following first blade harmonics (in degrees) were measured in the flight test, as shown in Table 1.

This particular flight condition has also been studied by Ahmad and Duque.[16] In their calculations, the blade collective was corrected to match the measured value of thrust. With no further trim, the rotor moments were approximately balanced in roll, but were out of balance in pitch. In the present hybrid analysis, the collective pitch was adjusted to match the measured overall thrust. To eliminate the rolling and pitching moment, the lateral and longitudinal cyclic pitch angles were also trimmed manually. The first blade harmonics (in degrees) after trimming are given in Table 1.

Figures 8 and 9 show the computed and measured pressure coefficients at several azimuthal and radial locations, applying the rigid wake model. At the inboard radial station $0.6R$, the suction peak on the advancing side compares fairly well with the measurements. However, the suction peak at $\psi = 180$ deg is underpredicted. This may again be due to the inadequacy of the coarse grid around radial station $0.6R$. The surface pressure distributions at the outboard radial station $0.91R$ compare well with the measured data on both the advancing and the retreating side. The lower surface pressures are consistently slightly underpredicted. At a number of radial stations, an irregular behavior near the leading-edge region can be seen, particularly near the 90-deg azimuthal angle. Ahmad and Duque[16] also reported similar behavior at the leading edge. Further investigation showed that at these locations, there were clear discontinuities in the first, C^1, and second, C^2, derivatives of the coordinates. Smoothing of these discontinuities would remove the pressure discontinuities; however, it then does not permit direct comparison with the earlier computational results, which include integrated values. Therefore, the discontinuities were not corrected for this study.

Figure 10 compares the computed normal load data with the measured airloads. There are four curves in the plot in Fig. 10. The results using the same first blade harmonics as the flight-test data, and the trimmed cyclic pitching angle, are both plotted. These results are

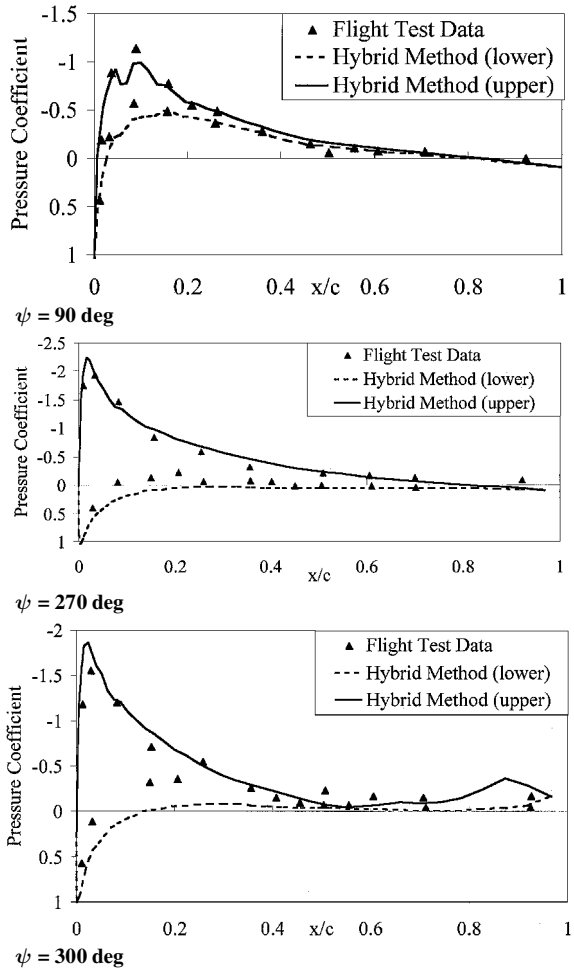

Fig. 9 Pressure coefficients at $r = 91\%R$ for advancing AH-1G rotor.

compared with flight-test data and the numerical results by Ahmad and Duque.[16]

Although several significant effects such as the influence of the fuselage, the hub, and the blade elastic deformations are neglected, the overall load and surface pressure derived by the hybrid method agree fairly well with flight-test data. At the retreating side near 270 deg, a variation in loads similar to the experiment is captured. Near the tip, the loads computed by hybrid method without trimming are overpredicted. After trimming to near-zero rolling and pitching moments, the computed loads indeed match better with flight-test data, except at the inboard section at $60\%R$.

AH-1 Low-Speed Descent

This case corresponds to a one-seventh scale model of the AH-1 rotor system experimentally tested by Splettstoesser et al.[36] The AH-1G/OLS rotor has a rectangular planform with BHT-540 sections. To accommodate full-scale pressure instrumentation, the airfoil section was slightly modified and resulted in a 9.71% thickness. The rotor is 1.916 m in diameter and has a 10.39-cm chord. The blade has a linear twist of 8.2 deg, and the blade root cutout is at $0.182R$.

The test condition studied corresponds to a low-speed descending flight at an advance ratio of 0.164. The tip Mach number is 0.664, and the overall thrust coefficient is 0.0054.

The blade dynamic motion information is extracted from Ref. 37. Table 2 shows the general blade motion coefficients. The rotor shaft angle is at zero degrees with respect to the freestream.

In the calculation by Strawn et al.,[37] the precone angle and the first harmonic flapping are fixed by the value in Table 2 from experiment. The collective and cyclic pitch angles are adjusted to match the experimental overall thrust coefficient, and they achieve zero pitching and rolling moments at the hub when the blade loads are integrated

Table 2 Blade dynamic motion of AH-1 rotor[37]

Blade motion	Value
θ_0	6.14
θ_{1s}	−1.39
θ_{1c}	0.9
β_{1s}	0.0
β_{1c}	−1.0
β_0	0.5

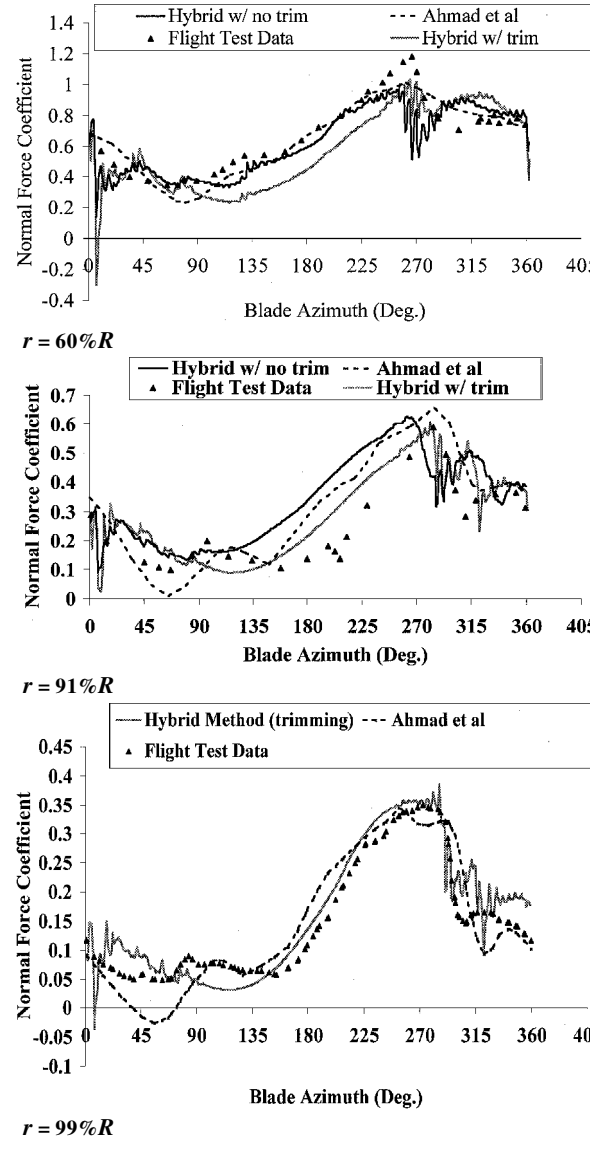

Fig. 10 Sectional thrust for the AH-1G rotor.

over the rotor disk. The present calculations use the same pitching and flapping angles as Table 2, except that the collective pitch angle was slightly modified to match the overall thrust coefficient. Thus, no trim loops were required for this calculation.

A multiblock H–O grid is used with clustering near the blade tip, leading, and trailing edges. The grid system spans 90 deg along the azimuthal direction and consists of 90, 43, and 80 cells in the chordwise, spanwise, and normal directions, respectively. Although a formal grid study was not performed for these calculations, similar studies[18,20] have shown this size grid to be appropriate for this computation.

The measured and computed pressure coefficients are compared on the advancing side in Fig. 11. The experiments provide the surface pressure measurements only on the rotor upper surface. The

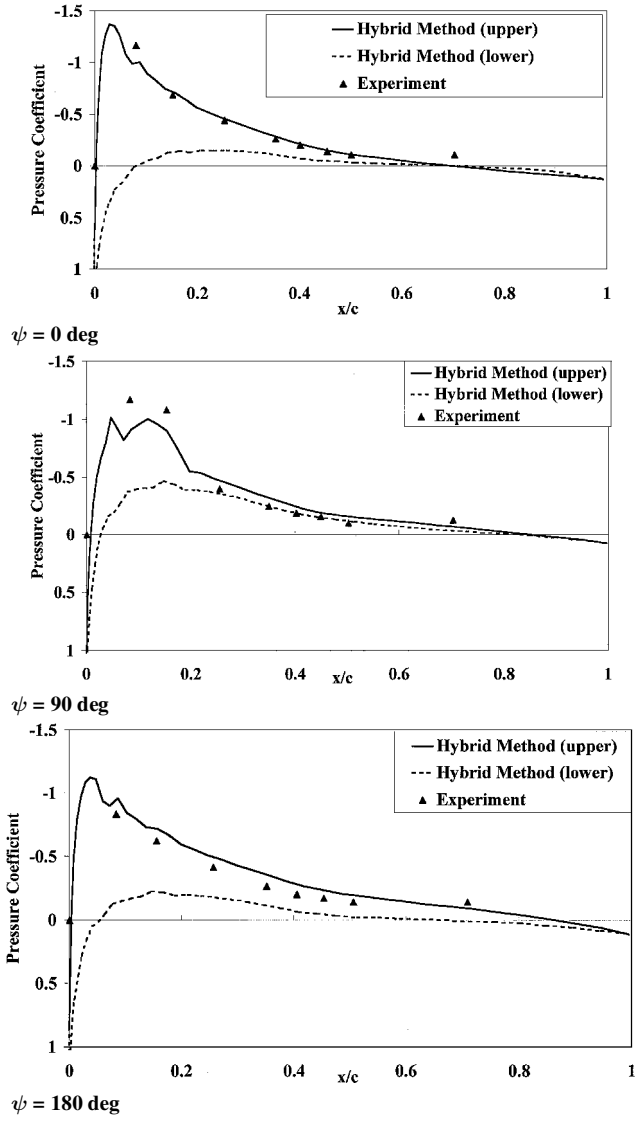

Fig. 11 Pressure coefficients at $r = 95.5\%R$ for an advancing AH-1G rotor with BVI.

computed results are in reasonably good agreement with the experimental values. The irregular behavior near the leading-edge region on the upper surface is still present, attributable to the errors in the airfoil coordinates.

The differential pressure coefficients near the leading edge of the rotor blade at 0.03 chord are plotted in Fig. 12. The results computed by Strawn et al.[37] include a comparable size Navier–Stokes grid to the hybrid method (coarse grid), as well as a finer Navier–Stokes grid applied to better approximate the wake (fine grid). These, along with the experimental data, are compared with the values computed from the hybrid method. As expected, the Strawn et al. fine grid does the best job at capturing the physics of the rotor on the first and last quadrants, but is comparable to the hybrid method in the two middle quadrants. Although the hybrid method misses some of the rapid changes in the flow, the location of the rapid pressure drop on the retreating side due to blade–vortex interaction is predicted.

Computational Resources

Computational resource requirements were compared for the hybrid and conventional Navier–Stokes methods for the UH-60A rotor. These results are compared in Table 3. The Navier–Stokes analysis requires that the grid model the entire rotor, whereas the hybrid method can be utilized to model only one rotor blade with the influence of the other blades modeled as a set of bound and tip vortices. Thus, there is a significant savings of 75% of the required grid in the hybrid method. For a single blade, the hybrid method provides, for the same grid, a 38% savings in CPU time. For a comparison of the full systems over two revolutions, the hybrid method provides a savings of approximately 84.5% over a full Navier–Stokes methodology.

Table 3 Comparison of CPU time for the Navier–Stokes and hybrid methods

Hybrid method, (grid size: 310,000; 1 blade)	Conventional Navier–Stokes method (grid size: 310,000 per blade; 4 blades)
Time/step, s	
Navier–Stokes (39% total grids): 8	80
Full potential (61% total grids): 3	
wake update (every 100 steps):	
1.4 per step total: 12.4	
Total number of time steps (two revolutions)	
14,400	14,400
Total CPU time, h	
49.6	320

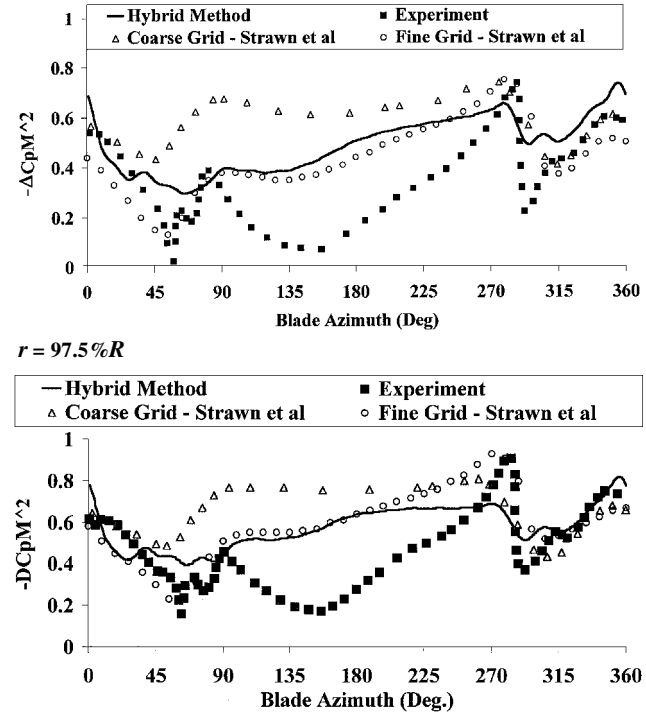

Fig. 12 Differential pressures near the leading edge ($x/C = 0.03$) of the AH-1G rotor.

Conclusions

A hybrid method has been developed for modeling aerodynamics of rotors in forward flight. Blade loads are comparable to full Navier–Stokes methods, but the present hybrid method requires significantly less computational memory and time. As demonstrated for the AH-60A rotor, the hybrid method can provide a comparable simulation at 25% of the number of grid points and about 15.5% of the CPU time requirements of the full Navier–Stokes simulation. Blade motion is modeled using experimental values and improves the blade load accuracy. Trim is still an expensive computation, but a loosely coupled methodology is shown to be successful in improving the blade loads while remaining cost effective.

References

[1]Johnson, W., "Development of a Comprehensive Analysis for Rotorcraft, I. Rotor Model and Wake Analysis," *Vertica*, Vol. 5, No. 2, 1981, pp. 90–130.

[2]Johnson, W., "Development of a Comprehensive Analysis for Rotorcraft, II. Aircraft Model, Solution Procedure and Applications," *Vertica*, Vol. 5, No. 3, 1981, pp. 185–216.

[3]Chattot, J. J., "Calculation of Three-Dimensional Unsteady Transonic Flows Past Helicopter Blades," NASA TP 1721, Oct. 1980.

[4]Sankar, L. N., and Prichard, D., "Solution of Transonic Flow Past Rotor Blades Using the Conservative Full Potential Equation," AIAA Paper 85-5012, Oct. 1985.

[5]Strawn, R. C., and Caradonna, F. X., "Numerical Modeling of Rotor Flows with a Conservative form of the Full Potential Equation," AIAA Paper 86-0079, July 1986.

[6]Strawn, R. C., and Tung, C., "The Prediction of Transonic Loading on Advancing Helicopter Rotors," NASA TM-88238, 1986.

[7]Strawn, R. C., Desopper, A., Miller, J., and Jones, A., "Correlation of PUMA Airloads—Evaluation of CFD Prediction Methods," *Proceedings of the 15th European Rotorcraft Forum*, American Helicopter Society, Sept. 1989.

[8]Sankar, L. N., and Tung, C., "Euler Calculations for Rotor Configurations in Unsteady Forward Flight," *Proceedings of the 42nd Annual Forum of the American Helicopter Society*, AHS International, Alexandria, VA, 1986.

[9]Steinhoff, J. S., and Ramachandran, K., "A Vortex Embedding Method for Free Wake Analysis of Helicopter Blades in Hover," *Proceedings of the 13th European Rotorcraft Forum*, American Helicopter Society, Paper 2-11, Sept. 1987.

[10]Steinhoff, J., and Ramachandran, K., "Free Wake Analysis of Compressible Rotor Flows," *AIAA Journal*, Vol. 28, No. 3, 1990, pp. 426–431.

[11]Ramachandran, K., Sclechtriem, S., Caradonna, F. X., and Steinhoff, J., "The Application of Vorticity Embedding to the Computation of Advancing Rotor Flows," *Proceedings of the American Helicopter Society 49th Annual Forum*, AHS International, Alexandria, VA, 1993.

[12]Ramachandran, K., and Caradonna, F. X., "The Use of CFD for Free-Wake Computation of Flows over General Multi-Blade Rotors," *American Helicopter Society Specialists' Meeting on Aeromechanics Technology and Product Design for 21st Century*, American Helicopter Society, Oct. 1995.

[13]Srinivasan, G. R., and Baeder, J. D., "TURNS: A Free Wake Euler/Navier–Stokes Numerical Method for Helicopter Rotors," *AIAA Journal*, Vol. 31, No. 5, 1993, pp. 959–962.

[14]Hariharan, N., "High Order Simulation of Unsteady Compressible Flows over Interacting Bodies with Overset Grids," Ph.D. Dissertation, Aerospace Engineering, Georgia Inst. of Technology, Atlanta, GA, Aug. 1995.

[15]Bangalore, A., and Sankar, L. N., "Forward Flight Analysis of Slatted Rotors Using Navier–Stokes Methods," AIAA Paper 96-0675, Jan. 1996.

[16]Ahmad, J., and Duque, E. P. N., "Helicopter Rotor Blade Computation in Unsteady Flows Using Moving Embedded Grids," AIAA Paper 94-1922, June 1994.

[17]Bauchau, O. A., and Ahmad, J. U., "Advanced CFD and CSD Methods for Multidisciplinary Applications in Rotorcraft Problems," *Proceedings of the AIAA/NASA/USAF Multidisciplinary Analysis and Optimization Symposium*, AIAA, Reston, VA, 1996, pp. 945–953.

[18]Berezin, C. R., and Sankar, L. N., "An Improved Navier–Stokes/Full Potential Coupled Analysis for Rotors," *Mathematical Computational Modeling*, Vol. 19, Nos. 3/4, 1994, pp. 125–133.

[19]Sopher, R., and Hallock, D. W., "Time History Analysis for Rotorcraft Dynamics Based on a Component Approach," *Journal of the American Helicopter Society*, Vol. 31, No. 1, 1986, pp. 43–51.

[20]Berkman, M. E., Sankar, L. N., Berezin, C. R., and Torok, M. S., "Navier–Stokes/Full Potential/Free-Wake Method for Rotor Flows," *Journal of Aircraft*, Vol. 34, No. 5, 1997, pp. 635–640.

[21]Mello, O. A., "An Improved Hybrid Navier–Stokes/Full-Potential Method for Computation of Unsteady Compressible Viscous Flows," Ph.D. Dissertation, Aerospace Engineering, Georgia Inst. of Technology, Atlanta, GA, Nov. 1994.

[22]Moulton, A. M., Hafez, M. M., and Caradonna, F. X., "Zonal Procedure for Predicting the Hovering Performance of a Helicopter," *ASME Journal*, Boundary Layer and Free Shear Flows, ASME Fluids Div., Vol. 184, 1994, pp. 151–162.

[23]Moulton, A. M., Hafez, M. M., and Caradonna, F. X., "The Development of a Hybrid CFD Method for the Prediction of Hover Performance," *American Helicopter Society Specialists' Meeting on Aeromechanics Technology and Product Design for 21st Century*, AHS, Paper 6-46, Oct. 1995.

[24]Moulton, M. A., Bridgeman, J. O., and Caradonna, F. X., "Development of an Overset/Hybrid CFD Method for the Prediction of Hovering Performance," *Proceedings of 53rd Annual Forum of the American Helicopter Society*, AHS International, Alexandria, VA, 1997.

[25]Bangalore, A. K., Moulton, M. A., and Caradonna, F. X., "The Development of an Overset/Hybrid Method for Rotorcraft Applications," *American Helicopter Society Specialists' Meeting for Rotorcraft Aerodynamics and Aeroacoustics*, AHS, Oct. 1997.

[26]Sankar, L. N., Malone, J. B., Tassa, Y., "An Implicit, Conservative Algorithm for Steady and Unsteady Transonic Potential Flows," *Proceedings of the AIAA 5th Computational Fluid Dynamics Conference*, AIAA Paper 81-1016, New York, 1981, pp. 199–212.

[27]Sankar, L. N., Bharadvaj, B. K., and Tsung, F.-L., "Three-Dimensional Navier–Stokes/Full Potential Coupled Analysis for Transonic Viscous Flow," *AIAA Journal*, Vol. 31, No. 10, 1993, pp. 1857–1862.

[28]Amirouche, F. M. L., *Computational Methods in Multibody Dynamics*, Prentice–Hall, Upper Saddle River, NJ, 1992.

[29]Smith, M. J., "A Fourth-Order Euler/Navier–Stokes Prediction Method for the Aerodynamics and Aeroelasticity of Hovering Rotor Blades," Ph.D. Dissertation, Aerospace Engineering, Georgia Inst. of Technology, Atlanta, GA, Feb. 1994.

[30]Stephens, C. H., Arena, A. S., Jr., Gupta, K. K., "Application of the Transpiration Method for Aeroservoelastic Prediction Using Computational Fluid Dynamics," *Proceedings of the 39th AIAA/ASME/ASCE/AHS Structures, Structural Dynamics, and Materials Conference*, Vol. 4, AIAA, Reston, VA, 1998, pp. 3092–3099.

[31]Mello, O. A. F., Prasad, J. V. R., Sankar, L. N., and Tseng, W., "Analysis of Helicopter/Ship Aerodynamic Interactions," *American Helicopter Society Aerodynamics Specialists Conference*, AHS, Jan. 1994.

[32]Johnson, W., *Helicopter Theory*, Dover, New York, 1994, pp. 469–547.

[33]Lorber, P. F., Stauter, R. C., and Landgrebe, A. J., "A Comprehensive Hover Test of the Airloads and Airflow of an Extensively Instrumented Model Helicopter Rotor," *Proceedings of 45th Annual Forum of the American Helicopter Society*, AHS International, Alexandria, VA, 1989.

[34]Lorber, P. F., "Aerodynamic Results of a Pressure Instrumented Model Rotor Test at the DNW," *Journal of American Helicopter Society*, Vol. 36, No. 4, 1991, pp. 66–76.

[35]Cross, J. L., and Watts, M. E., "Tip Aerodynamics and Acoustics Test: A Report and Data Survey," NASA-RP-1179, NASA Ames Research Center, Dec. 1988.

[36]Splettstoesser, W. R., Schultz, K. J., Boxwell, D. A., and Schmitz, F. H., "Helicopter Model Rotor–Blade Vortex Interaction Impulsive Noise: Scalability and Parametric Variations," *Proceedings of the 10th European Rotorcraft Forum*, American Helicopter Society, Aug. 1984.

[37]Strawn, R. C., Duque, E. D. N., and Ahmad, J., "Rotorcraft Aeroacoustics Computations with Overset-Grid CFD Methods," *Journal of the American Helicopter Society*, Vol. 44, No. 2, 1999, pp. 132–140.